

A deep learning based 2-dimensional hip pressure signals analysis method for sitting posture recognition

Zhe Fan ^a, Xing Hu ^{a,*}, Wen-Ming Chen ^{b,*}, Da-Wei Zhang ^{a,*}, Xin Ma ^c

^a School of Optical-electrical Information and Computer Engineering, University of Shanghai for Science and Technology, 516, JunGong Road, Shanghai, PR China

^b Academy for Engineering & Technology, Fudan University, 220 Handan Road, Shanghai, PR China

^c Department of Orthopaedics, Huashan Hospital, Fudan University, 12 Middle Wulumuqi Road, Shanghai, PR China

ARTICLE INFO

Keywords:

Sitting posture

Hip pressure

2D pressure sensor array

Convolution neural network

ABSTRACT

Abnormal sitting postures usually cause adolescents' myopia, scoliosis, and degenerative diseases. Therefore, research on intelligent monitoring technology that can quickly and accurately identify irregular sitting postures is of profound significance to the healthy development of adolescents. Existing methods mostly use computer vision to recognize sitting posture, but the model is not only complicated but also easily interfered with by problems such as occlusion and light. This paper proposes a method based on the analysis of the pressure on the hip interface to identify the sitting postures. An array pressure sensor placed on the cushion collects the tester's hip pressure and obtains a pressure heat map. This paper uses traditional feature extraction and shallow classifier methods and popular end-to-end deep convolutional neural network (CNN) methods to identify different types of sitting postures. The method in this paper is verified on the data of multiple testers of different body types. Experimental results show that the classification accuracy based on CNN reaches 99.82%, which proves the effectiveness of the method in sitting posture recognition. The study indicated hip pressure distribution is closely related to the sitting posture, and compared with computer vision, it is less disturbed and easier to recognize. The time efficiency of feature extraction using CNN is nearly 30% higher than traditional methods. Therefore, in the practical application of real scenes, with the increase of data volume, the time benefit brought by CNN can be more considerable and our system can be embedded in the cushion and do real-time detection.

1. Introduction

At present, long-term intense study often requires adolescents to maintain a prolonged sitting posture, which can last for a half day or more in a day [1,2]. However, because adolescents are in the physical development stage, various sitting positions that remain relatively unchanged, irregular, or even wrong for a long time, such as left and right deflection, hunchback, sitting back, etc., tend to cause adverse effects on their blood and respiratory system [3], the psoas muscle activity [4], the natural curve of the spine [5], vision and mood [6], etc. In particular, the number of adolescents with scoliosis is increasing year by year. According to statistics, there are currently more than 3 million patients with scoliosis in our country, and the number is increasing at an annual rate of 300,000. More than half of them are teenagers, and the most common are among adolescents aged 8 to 14. And it is clinically found that the occurrence of adolescent scoliosis is closely associated with posture. Therefore, timely and accurate identification of irregular sitting

posture and timely correction of the sitting posture is important issues that concern the healthy development of adolescents [7,8].

In the medical and health field, sitting posture recognition and correction have a wide range of applications and huge market opportunities, and various sitting posture detection systems are also constantly appearing. At present, there are two principal ways of sitting posture recognition. One is to take a camera to collect images of the tester and recognize the posture [9,10]. However, methods based on computer recognition are susceptible to interference from factors such as viewing angles, light, and occlusion, and are not conducive to the privacy protection of testers. Another way is tantamount to sense the abnormality of the sitting posture by sensing the pressure on the hips, back, or chest through a pressure sensing system. For example, LifeChair designed by Ishac and Suzuki [11] detects the sitting posture of the subject by analyzing the pressure data collected by the force sensor in the cushion. Kim *et al.* [12] designed a smart chair that uses an 8 × 8 matrix pressure sensor based on a force-sensitive resistor (FSR) of PET

* Corresponding authors.

E-mail addresses: huxing@usst.edu.cn (X. Hu), chenwm@fudan.edu.cn (W.-M. Chen), dwzhang@usst.edu.cn (D.-W. Zhang).

film to collect the pressure data of the subject's buttocks. Since hip pressure is directly related to the sitting posture and suffers less interference, it is easier and less perceptible to recognize sitting posture than computer vision-based methods.

As the types of sensors increase, the choice of various classification algorithms also affects the accuracy of sitting posture recognition to a great extent. Wan *et al.* [13] used a support vector machine (SVM) to classify the four sitting postures by a 32×32 hip pressure sensor array, and finally achieved an accuracy of 89.6%. Ahmad *et al.* [14] used a decision tree algorithm to classify the pressure sensor data from a 4×4 matrix, and the accuracy of the classification of the four sitting postures reached 80%. Benocci [15] *et al.* used a K-Nearest Neighbor (KNN) classifier to classify wearable multi-sensor device data based on 32-bit ARM Cortex M3 architecture, with an accuracy rate of 93.7%. Jongryun *et al.* [16] used a radial basis function kernel support vector machine, and the final accuracy rate reached 97.94%. This article uses two methods to analyze the 2D pressure signal. The first is to apply the traditional SVM classifier similar to the work by [13], but we use handcrafted features and learned features respectively, and make comparison. Experiments show that the learned features based on PCA achieve a higher accuracy rate. The second is to use methods based on popular deep learning to build a CNN model to achieve end-to-end automatic recognition of human sitting posture. In contrast, other studies focused on the analysis and processing of hip pressure distribution. More importantly, the automatic processing of data can make the sitting posture recognition system have efficient real-time performance when processing different test targets.

2. Materials and methods

2.1. The pressure acquisition system

The acquisition of buttock pressure distribution at different sitting posture was achieved by using a film-type piezoresistive sensor array and the dedicated data acquisition circuit.

The sensor shown in Fig. 1 is a 44×52 pressure sensor array with an effective sensing area of $306 \times 362 \text{ mm}^2$. The thickness of the sensor is about 0.5 mm, with a total of 2288 independent sensing units. The

circuit board is mainly composed of 12 LM324 chips as the main control chip, 8 74HC4052 chips and 7 74HC4051 chips, for the purpose of collection, processing and transmission of pressure data. The sensor is connected to the circuit board through four FPC lines and the data were then fed into the PC computer through a USB port. The sampling frequency of the system is 15 Hz, and the raw output data from each sensor is an 8-bit binary values proportional to the regional pressure. A graphical toolkit (Qt Design Studio) was utilized to construct the host computer software and interactive interface to realize the continuous collection and visualization of the pressure distribution data from the subjects' buttocks for different sitting postures.

The sensor uses line-rank scanning method to read the raw data of each pressure sensing unit. When the sensing unit is subjected to external force and the resistance changes, the resistance output can be selected by multiple analog switches after resistance-to-voltage and operational amplification. After the analog switch is turned on, it can be connected to the analog to digital conversion (ADC) acquisition channel of the main control chip. After transmission, the final voltage data can be obtained through the internal ADC processing of the chip. By amplifying the voltage signal, the system will eventually display the pressure distribution of cloud images.

2.2. Dataset

2.2.1. Considered postures

Since there is no significant difference in hip pressure images between different genders of the same weight and height, on the contrary, there are significant differences between different weight. Therefore, this study selected 8 male subjects of different ages and heights with a large weight coverage. Its basic body data is shown in Table 1.

In this study, 5 different sitting postures were set up, namely backward, forward, left, right, and standard sitting postures. Table 2 shows the type and detailed description of each sitting posture. In order to ensure the universality of these postures, we asked the subjects to sit on a chair with a height of 40 cm, and the body can perform reasonably movements in the usual state within a certain angle.

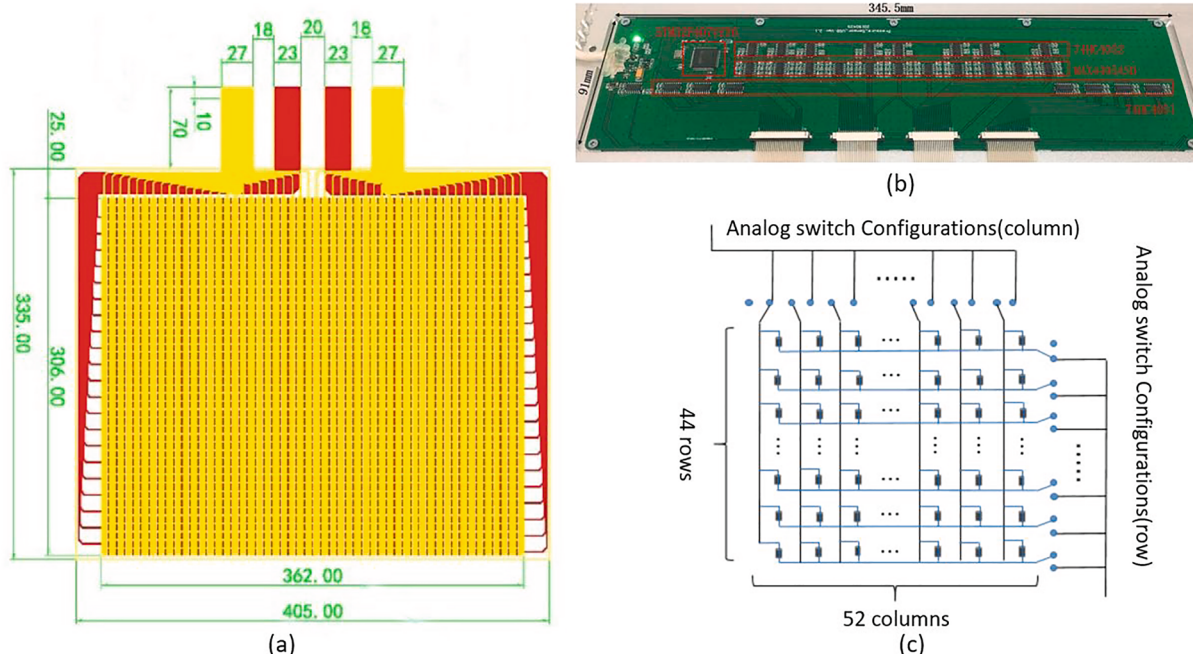


Fig. 1. (a) The size of the pressure sensor array used in buttock pressure measurements (Unit: mm); (b) the layout of the circuit board for pressure data acquisition; (c) schematics of the ADC scanning circuit for each individual sensing unit. (single-column fitting image).

Table 1
Essential Information of subjects.

Subject Number	Age (years old)	Weight(kg)	Height(cm)
1	24	70	179
2	21	69	171
3	40	63.5	168
4	26	74.3	169
5	25	73	176
6	24	74	178
7	24	89	178
8	37	130	190

Table 2
List of Recorded Postures.

Posture	Description
Leaning Back	The center of gravity shifts to the lower back. In most cases, the center of gravity of the lumbar spine is suspended in the air.
Leaning Forward	The center of gravity moves forward, usually manifested as a significant hunchback and forward tilt of the cervical spine
Leaning Left	The center of gravity moves to the left, usually in the form of warped legs, which can support the weight of the main body with the left arm.
Leaning Right	The center of gravity shifts to the right, usually in the form of a raised leg, and the right arm supports the weight of the main body.
Standard	The tester keeps the upper body upright and keeps the body relaxed.

2.2.2. Acquisition process

After specifying all types of sitting postures, in order to obtain better data, we adopted a hard seat without armrests. When collecting non-

standard posture data, we asked each subject to pose in a non-standard posture for about 10 s, and then fine-tune the posture within a certain angle range for about 25 s. At the same time, the sampling frequency of the pressure image acquisition device is set to about 4 Hz, and finally, each person will collect about 140 pictures in .png format per posture. Fig. 2 shows example images of pressure in different postures.

2.3. Experiments

2.3.1. SVM with handcrafted feature

The gray-level co-occurrence matrix (GLCM) is a widely recognized image texture feature processing method, which has strong discrimination ability and good robustness. GLCM can reflect the comprehensive information of the image gray level on the direction, adjacent interval, and change range, and is the basis for analyzing the local patterns of the image and their arrangement rules. Haralick *et al.* [17] initially proposed a total of 14 different statistical features, but the overall calculation process was time-consuming so that many scholars have tried to improve these features. Ulaby *et al.* [18] found that among the 14 statistical features obtained by GLCM, only contrast, correlation, energy and inverse difference moment (IDM) were not correlated, and these four statistical features could provide a satisfactory classification effect; Baraldi *et al.* [19] concluded that entropy and contrast were the two statistical features with the greatest degree of difference among the 14 statistical features. Therefore, based on the above research, in order to reduce the amount of calculation and get higher classification accuracy, we choose 4 of the statistics based on GLCM as the feature matrix, including energy, entropy, contrast, and inverse difference moment

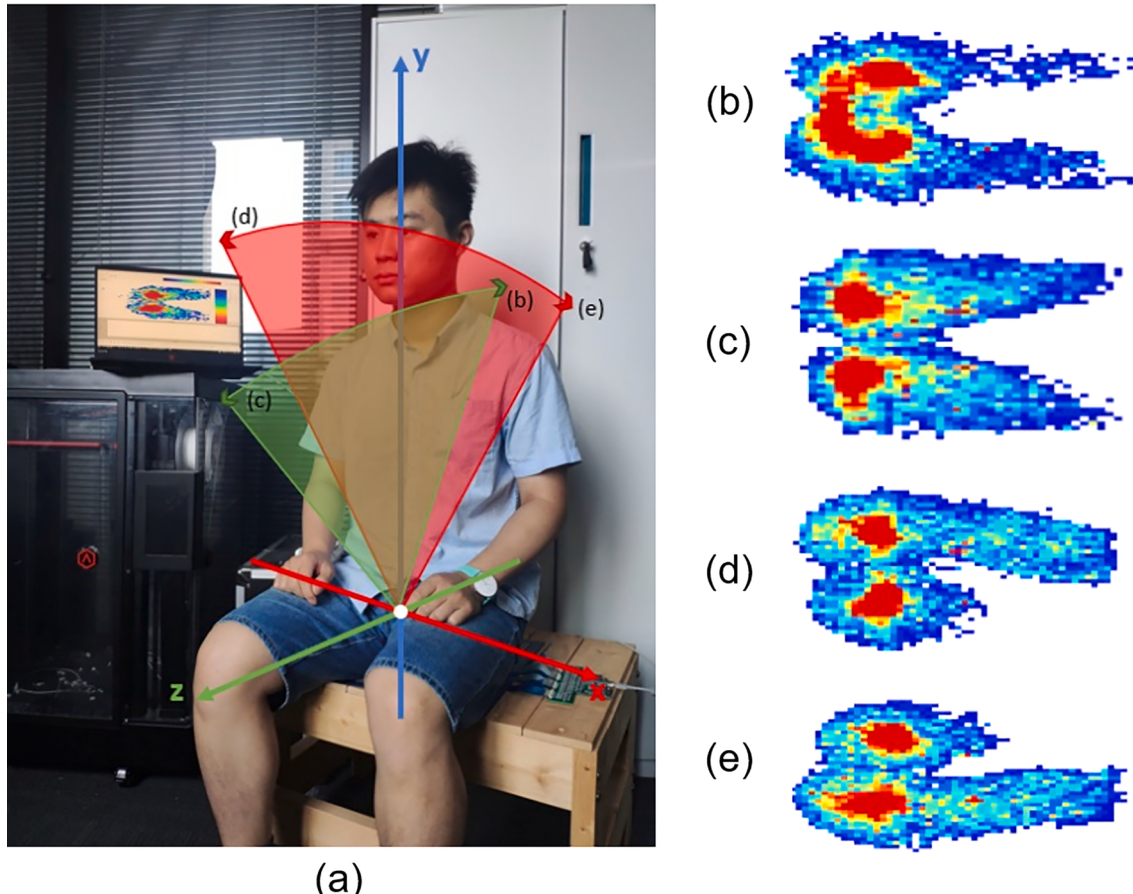


Fig. 2. The experimental setup for obtaining interfacial pressures from the subject's buttock at different sitting posture (a), and typical pressure distributions (i.e., heat map) were shown for leaning backward (b), forward(c), right (d) and left (e) deviating from the standard sitting posture. (single-column fitting image).

(IDM), which are defined as:

$$\text{Energy} = \sum_i \sum_j P(i,j)^2 \quad (1)$$

$$\text{Entropy} = \sum_i \sum_j P(i,j) \log(i,j) \quad (2)$$

$$\text{Contrast} = \sum_i \sum_j P(i,j) |i - j|^2 \quad (3)$$

$$\text{IDM} = \sum_i \sum_j \frac{P(i,j)}{1 + |i - j|^2} \quad (4)$$

Regarding the parameters above:

- Energy reflects the uniformity of the image gray distribution and the fineness of the texture
- Entropy reflects the complexity of the image
- Contrast reflects the sharpness of the image and texture
- IDM reflects the clarity and regularity of the texture.

In our research, we use the statistics extracted by GLCM as a matrix as a manual feature, and we add a non-linear kernel to the support vector machine to improve performance. We choose Gaussian RBF kernel, which can be expressed as:

$$k(x, x') = \exp\left(-\frac{\|x - x'\|^2}{2\sigma^2}\right) \quad (5)$$

In this study, we set $C = 20$ (a regularization parameter that can improve the generalization performance of SVM) and set $\sigma = 4.5$. In order to ensure the credibility of the results, we evaluated the model using hierarchical 5-fold cross-validation.

2.3.2. SVM with learned feature

To extract the learning features, we chose the principal component analysis (PCA) method. PCA is an unsupervised transformation method proposed by Karl *et al.* [20], which can extract relevant information and reduce the dimensionality of the original features. In practical applications, to reduce the data from k-dimension to n-dimension, the general method of principal component analysis is:

- Standardize the original data and transform it into k-dimensional data $X^T = (x_1, x_2, x_3, \dots, x_N)$;
- Calculate the covariance matrix:

$$\text{Cov} = \frac{\sum_{i=1}^k (x_i - \mu_x)^T (x_i - \mu_x)}{k - 1} \quad (6)$$

Where μ_x is the mean vector of the data.

- Calculate and set the eigenvectors and eigenvalues of the covariance matrix in decreasing order;
- Represent the projection matrix $P_{k \times n} = (p_1, p_2, p_3, \dots, p_n)$ based on the eigenvectors;
- The results of dimensionality reduction is:

$$Y = XP \quad (7)$$

In our experiment, we apply the PCA method to the training set and test set shown in Fig. 3 and set the target dimension of dimensionality reduction to 3. Fig. 4 shows the visualization results of PCA, and also shows that the five sitting postures can be easily separated, which means that PCA can successfully extract the principal component features and ensure that a small amount of original data is lost.

Then we use the support vector machine and Radial Based Function (RBF) kernel to complete the classification task, and use the grid search method to find the optimal parameters, including regularization parameters and σ . The grid search method can help us obtain the highest classification accuracy.

2.3.3. CNN-Based classifier

Since the deep learning network can efficiently extract the effective features of the data, this method has been widely used in image processing tasks such as image classification [21,22], recognition [23] and anomaly detection [24]. In the convolutional layer of a CNN, one neuron is only connected to some neighboring neurons. A convolutional layer of CNN usually contains several feature maps and each feature map is composed of some neurons arranged in rectangles. The neurons of the same feature plane share weight, and the shared weight here is the core.

In the task of sitting posture recognition, we established a model based on CNN to train and classify the five postures in Table 2. The network architecture of our model is shown in Fig. 5.

The parameters corresponding to the 2-dimensional CNN model structure we used are shown in Table 3. The CNN model has 2 convolutional layers, 2 max-pooling layers, and 2 fully connected layers. The network input data size is $32 \times 32 \times 3$. After the convolutional layers and the max-pooling layers, the feature map is connected to the fully connected layers and process neural network classification on the extracted features to form the final output. The size of the convolution kernel is (3,3), the stride is (1,1), and both the activation functions of the convolutional layer and the fully connected layer use the Rectified Linear Unit (ReLU) function.

Training data pre-processing: For the collected data set, we get an image with an initial size of 1100×380 . Before training, the length of these images is adjusted to 32 pixels, and then the short sides are changed in the same proportion, and in order to obtain a square image, the rest is filled with RGB (255,255,255). For the split of training and test data sets, we divide the initial data set into 5 equal parts according to the same proportion of the 5 poses, and each part has 20% of the test data.

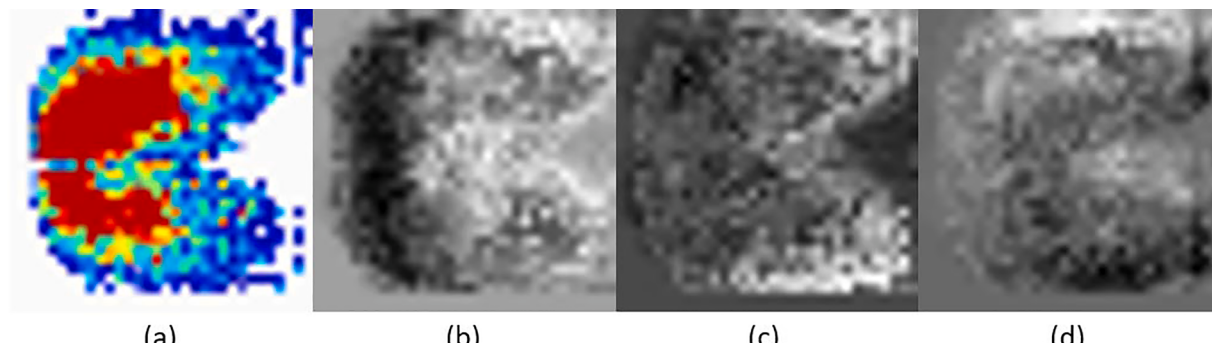


Fig. 3. (a) is the original data size as 32x32. (b)(c)(d) is the first 3 eigen images reconstructed based on eigenvectors after reducing the original dimension 1024 to 3. (single -column fitting image).

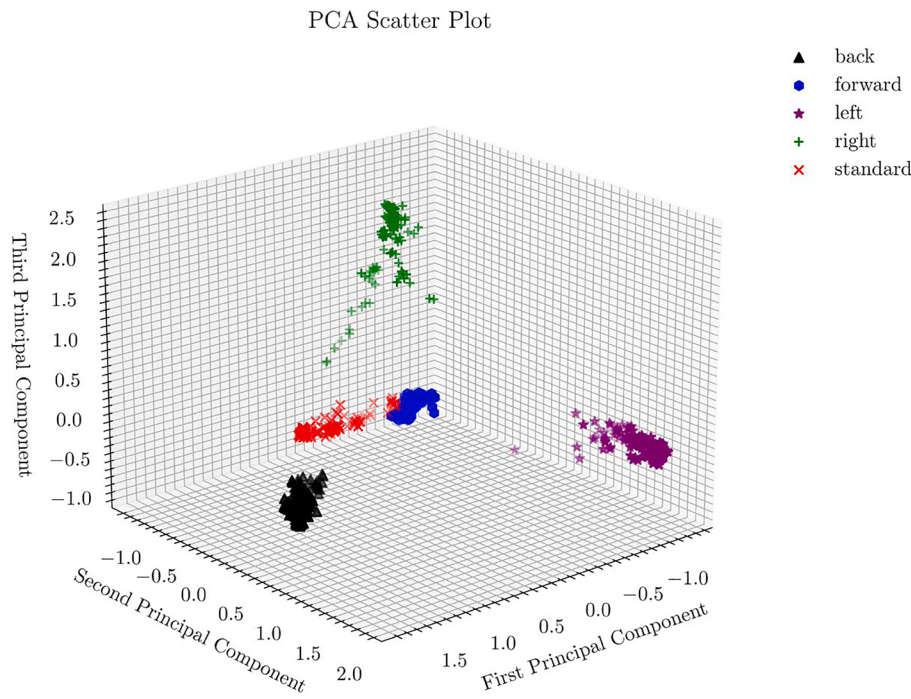


Fig. 4. The 3D scatter plot of the first three principal components of the PCA features for five different types of sitting posture. (2-column fitting image).

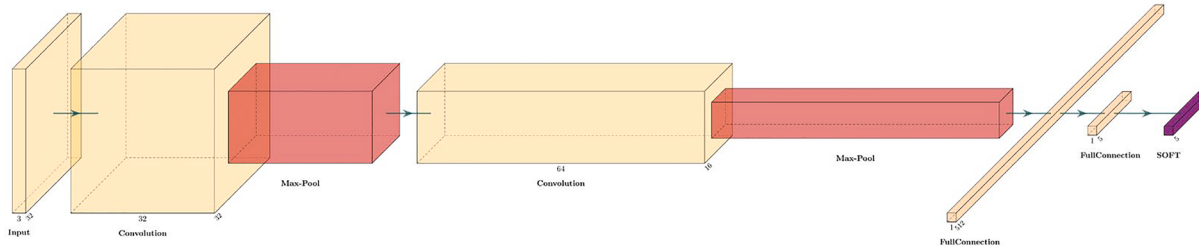


Fig. 5. The structure of the 7-layered CNN-based classifier. (2-column fitting image).

Table 3
Layers and parameters of 2-dimensional CNN model.

Layer	Kernel	Filters	Stride	Activation Function
Conv2D	(3,3)	32	(1,1)	Relu
Max-pooling2D	(2,2)	32	(2,2)	–
Conv2D	(3,3)	64	(1,1)	Relu
Max-pooling2D	(2,2)	64	(2,2)	–
Dense	512	–	–	Relu
Dense	5	–	–	Softmax

Training details: The input image size of the network is $32 \times 32 \times 3$. We use the TensorFlow framework and Python scripts running on NVIDIA GTX1060. The hyperparameters are set as: learning rate $\eta = 5e-5$, attenuation = $1e-6$. Each part of the data set is trained for 10 epochs. Fig. 6 shows the loss curve of the 5-fold training process, and the classification accuracy reaches about 100% after 10 epochs.

3. Results

3.1. Classification results

We enumerate a large number of candidate parameters, and use the grid search method to loop through all candidate parameters, try every possibility, and finally determine the optimal solution through the best-

performing parameter. Table 4 shows the optimal parameter sizes of SVMRBF under manual and learning features. We used training data composed of five sitting postures to train the traditional classifier and the deep learning classifier separately. The test data contain the remaining 20% of each posture, which is used to calculate the classification accuracy. Table 5 summarizes the accuracy of the different experiments in each compromise. Experimental results show that the average accuracy of the RBF kernel support vector machine based on GLCM is 92.48%, and its best accuracy is 94.509%. The average accuracy of the PCA-based RBF kernel support vector machine is 99.27%, and its best accuracy is 99.369%.

In deep learning, the average classification accuracy of our CNN model is 99.82%, and its best accuracy is 100%. After the experiment, use the confusion matrix shown in Fig. 7 to analyze the best part of the training model. The X-axis is the actual class, and the Y-axis represents the predictions performed by the model.

In Table 6, we compare the time taken by these three methods to process the test set we made in section 2.2. Considering that the biggest difference between CNN and traditional methods is that the logic and efficiency of feature extraction are different, so we focused on comparing the time spent on feature extraction. From the results in Table 6, it can be seen that the CNN feature extraction achieves the maximum efficiency, which is 30% higher than that of the PCA method. At the same time, in order to ensure the comparison of the results, we uniformly use the CPU for calculations, and the CNN method can also be

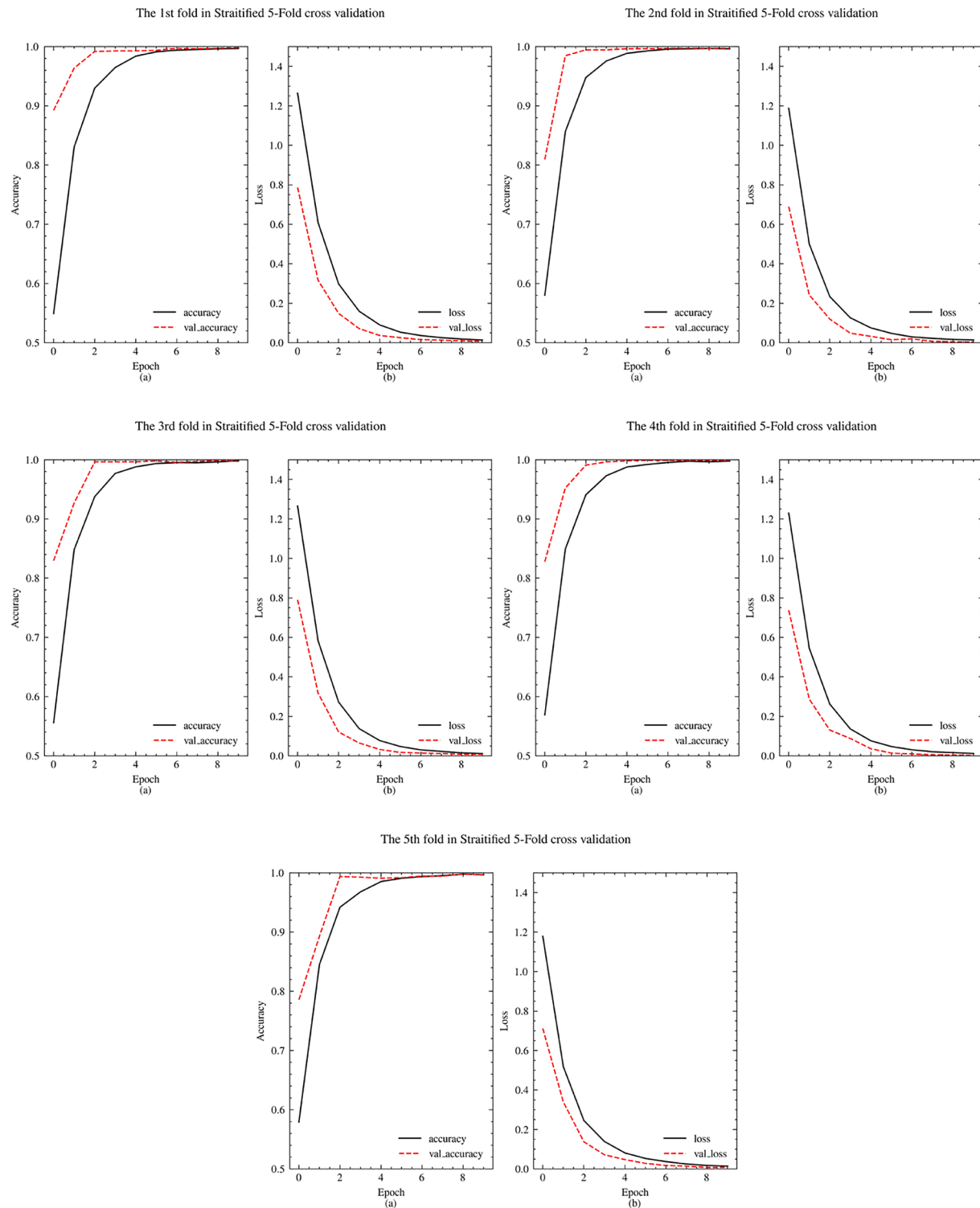


Fig. 6. The loss and accuracy curves in the training process. In each process, (a) is the curve of the accuracy of training and validation and (b) is the loss of training and validation. (2-column fitting image).

Table 4
The detailed results of stratified 5-Fold Cross-validation.

Method	Optimal Parameters
GLCM + SVM _{RBF}	C = 5e4, $\sigma = 0.2$
PCA + SVM _{RBF}	C = 1e5, $\sigma = 0.1$

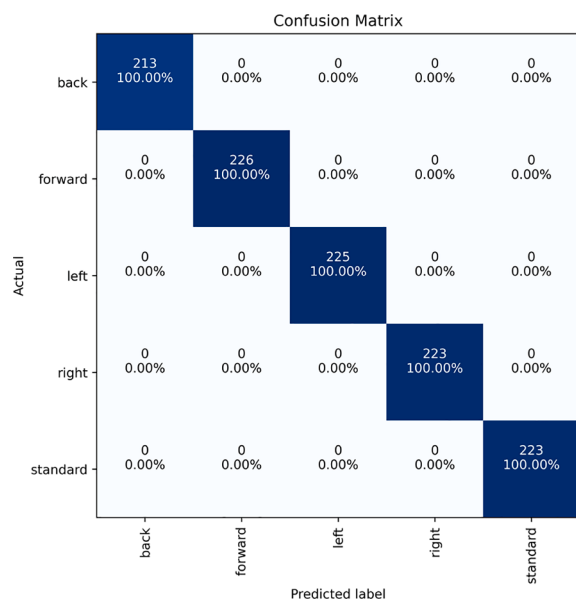
calculated on the GPU, which means that its calculation speed can be further improved.

In terms of complexity, the total parameters and Floating-Point Operations Per Second (FLOPs) are parameters that describe the time-complexity and memory-complexity of CNN model. And through the calculation of parameters of each layer in Table 3, it can be obtained that FLOPs of our CNN model during training are 4,238,029 and the number of parameters is 2,119,621. In the training process of PCA + SVM_{RBF}

Table 5

The detailed results of stratified 5-Fold Cross-validation.

Method	1	2	3	4	5	Mean Accuracy
GLCM + SVM _{RBF}	90.876%	91.606%	92.606%	92.793%	94.509%	92.48%
PCA + SVM _{RBF}	98.829%	99.006%	99.097%	99.369%	99.190%	99.29%
CNN	99.819%	99.729%	99.819%	100%	99.308%	99.82%

**Fig. 7.** The confusion matrix for the training set based on CNN mode. (1-column fitting image).**Table 6**

Time required to process a sequence of the test dataset using an Intel i7 2.21Ghz.

Method	Time	Time for each sample	Conditions
GLCM + SVM _{RBF}	3.96 s	356.44 ms	Time to extract features, this does not include time for classification
PCA + SVM _{RBF}	315.42 ms	284.4 μ s	–
CNN	219.97 ms	198.3 μ s	–

method, the SVM scales between $O(n_{features} \times n_{samples}^2)$ and $O(n_{features} \times n_{samples}^3)$, depending on how efficiently the cache is used in practice [25]. In addition, it can also be shown from the complexity of SVM that its computation and storage requirements will increase rapidly with the increase of the number of training vectors. Given that the application in real scenes is characterized by huge amount of data and complex dimension of feature vectors, CNN not only guarantees its extremely high accuracy, but the time benefit it brings is more considerable.

4. Discussion

After the sensor obtains the raw pressure data, it is converted into an image of hip pressure according to a preset sampling frequency. The preprocessing steps in section 2.3.3 are used for the original data to reduce the data size and improve the training speed. In order to further improve the speed of the learning phase, all data values have been normalized. Since PCA is usually used for dimensionality reduction of high-dimensional data, it can convert the original high-dimensional data into a low-dimensional space to make its variance as large as possible. However, if a certain characteristic value of the data is particularly large, it will have a great impact on the overall error calculation.

Therefore, we standardized the preprocessed data in the classification experiment based on the PCA method. Our 3 experiments used 80% of the entire data set for training, and the remaining 20% were used to verify the system. In order to ensure the universality of the results, all the sitting postures of the 8 subjects were divided equally into the training and validation data sets. Considering the negative factors such as the size of the data and the contingency of the random and even distribution of the data set, we conducted a hierarchical 5-fold cross-validation of the above three experiments to improve its generalization ability and ensure its effectiveness.

Specifically, the accuracy of PCA + SVM_{RBF} in the experiment is significantly higher than that of GLCM + SVM_{RBF}, which means that in the classification of hip pressure images, PCA can indeed extract effective low-dimensional features, so that SVM can complete the classification. However, from all experiments, CNN has the highest accuracy rate and compared to PCA, it can extract features faster and retain the original features as much as possible to prevent the loss of special features.

5. Conclusions

In this experiment, by comparing the traditional feature classifier and the deep learning classifier, the results we get show that the CNN model structure shown in Table 3 has the highest accuracy rate with 99.82% in our datasets. In addition, in order to better evaluate the recognition performance, the confusion matrix is also calculated. Besides, it can be shown in Table 6 that the framework is computationally very efficient, allowing for real-time processing and it is possible to substitute traditional methods. It is proven that CNN is better than traditional methods and has practical applications value which means that it can be embedded in the cushion and do real-time detection.

Considering that the five sitting postures we proposed still have limitations on monitoring and protecting the human spine. For example, different degrees of oblique postures have different degrees of damage to the human spine, and there is no need to correct irregular but harmless sitting postures. Therefore, for future versions, the recognition of sitting posture can be combined with the detection of spine curvature, which has stronger pertinence. In the future, we will explore the relationship between sitting posture and physical and mental fatigue by analyzing the time series of stress signal data.

CRediT authorship contribution statement

Zhe Fan: Methodology, Software, Validation, Formal analysis, Investigation, Writing – original draft, Data curation. **Xing Hu:** Methodology, Conceptualization, Validation, Writing – review & editing, Visualization, Supervision. **Wen-Ming Chen:** Conceptualization, Validation, Resources, Writing – review & editing, Visualization, Supervision. **Da-Wei Zhang:** Writing – review & editing, Visualization. **Xin Ma:** Writing – review & editing, Visualization.

Declaration of Competing Interest

The authors declare that they have no known competing financial interests or personal relationships that could have appeared to influence the work reported in this paper.

Acknowledgements

This work is supported by the national key research and development program (2019YFB1705702), Shanghai Technology and Science Funds (20531901000) and Medical Engineering Fund of Fudan University (yg2021-019).

References

- [1] A. Biswas, P.I. Oh, G.E. Faulkner, R.R. Bajaj, M.A. Silver, M.S. Mitchell, D.A. Alter, Sedentary time and its association with risk for disease incidence, mortality, and hospitalization in adults: a systematic review and meta-analysis, *Ann. Intern. Med.* 162 (2) (2015) 123–132, <https://doi.org/10.7326/M14-1651>.
- [2] A.J. Atkin, E. Adams, F.C. Bull, et al., Non-Occupational Sitting and Mental Well-Being in Employed Adults, *ann. behav. med.* 43 (2012) 181–188, <https://doi.org/10.1007/s12160-011-9325-6>.
- [3] J.L. Veerman, G.N. Healy, L.J. Cobiac, T. Vos, E.A. Winkler, N. Owen, D. W. Dunstan, Television viewing time and reduced life expectancy: a life table analysis, *Br. J. Sports Med.* 46 (13) (2012) 927–930, <https://doi.org/10.1136/bjsports-2011-085662>.
- [4] A.P. Claus, J.A. Hides, G.L. Moseley, P.W. Hodges, Different ways to balance the spine: subtle changes in sagittal spinal curves affect regional muscle activity, *Spine* 34 (6) (2009) E208–E214, <https://doi.org/10.1097/BRS.0b013e3181908ead>.
- [5] N.M. Dunk, J.P. Callaghan, Gender-based differences in postural responses to seated exposures, *Clinical biomechanics (Bristol, Avon)* 20 (10) (2005) 1101–1110, <https://doi.org/10.1016/j.clinbiomech.2005.07.004>.
- [6] A.L. Rebar, C. Vandelanotte, J. van Uffelen, C. Short, M.J. Duncan, Associations of overall sitting time and sitting time in different contexts with depression, anxiety, and stress symptoms, *Mental Health and Physical Activity* 7 (2) (2014) 105–110.
- [7] J.C. Cheng, R.M. Castelain, W.C. Chu, A.J. Danielsson, M.B. Dobbs, T.B. Grivas, C. A. Gurnett, K.D. Luk, A. Moreau, P.O. Newton, I.A. Stokes, S.L. Weinstein, R. G. Burwell, Adolescent idiopathic scoliosis, *Nat Rev Dis Primers* 1 (1) (2015), <https://doi.org/10.1038/nrdp.2015.30>.
- [8] H.R. Weiss, M.M. Moramarco, M. Borysov, S.Y. Ng, S.G. Lee, X. Nan, K. A. Moramarco, Postural Rehabilitation for Adolescent Idiopathic Scoliosis during Growth, *Asian spine journal* 10 (3) (2016) 570–581, <https://doi.org/10.4184/asj.2016.10.3.570>.
- [9] C. Juang, C. Chang, Human Body Posture Classification by a Neural Fuzzy Network and Home Care System Application, *IEEE Transactions on Systems, Man, and Cybernetics - Part A: Systems and Humans* 37 (6) (Nov. 2007) 984–994, <https://doi.org/10.1109/TSMCA.2007.897609>.
- [10] W. Song-Lin and C. Rong-Yi, “Human behavior recognition based on sitting postures,” 2010 International Symposium on Computer, Communication, Control and Automation (3CA), 2010, pp. 138-141, <https://doi.org/10.1109/3CA.2010.5533871>.
- [11] K. Ishac, K. Suzuki, LifeChair: A Conductive Fabric Sensor-Based Smart Cushion for Actively Shaping Sitting Posture, *Sensors (Basel, Switzerland)* 18 (7) (2018) 2261, <https://doi.org/10.3390/s18072261>.
- [12] W. Kim, B. Jin, S. Choo, C.S. Nam, M.H. Yun, Designing of smart chair for monitoring of sitting posture using convolutional neural networks, *Data Technologies and Applications* 53 (2) (2019) 142–155, <https://doi.org/10.1108/DTA-03-2018-0021>.
- [13] Q. Wan, H. Zhao, J. Li, P. Xu, Hip Positioning and Sitting Posture Recognition Based on Human Sitting Pressure Image, *Sensors (Basel, Switzerland)* 21 (2) (2021) 426, <https://doi.org/10.3390/s21020426>.
- [14] J. Ahmad, H. Andersson, J. Sidén, Sitting posture recognition using screen printed large area pressure sensors, *IEEE SENSORS* 2017 (2017) 1–3, <https://doi.org/10.1109/ICSENS.2017.8233944>.
- [15] M. Benocci, E. Farella, L. Benini, A context-aware smart seat, in: 2011 4th IEEE International Workshop on Advances in Sensors and Interfaces (IWASI), 2011, pp. 104–109, <https://doi.org/10.1109/IWASI.2011.6004697>.
- [16] J. Roh, H.-J. Park, K. Lee, J. Hyeong, S. Kim, B. Lee, Sitting Posture Monitoring System Based on a Low-Cost Load Cell Using Machine Learning[J], *Sensors* 18 (2) (2018) 208, <https://doi.org/10.3390/s18010208>.
- [17] R.M. Haralick, Statistical and structural approaches to texture, *Proc. IEEE* 67 (5) (May 1979) 786–804, <https://doi.org/10.1109/PROC.1979.11328>.
- [18] F. Ulaby, F. Kouyate, B. Brisco, T.H. Williams, Textural Information in SAR Images, *IEEE Trans. Geosci. Remote Sensing GE-24* (2) (1986) 235–245.
- [19] A. Baraldi, F. Pannigiani, An investigation of the textural characteristics associated with gray level cooccurrence matrix statistical parameters, *IEEE Trans. Geosci. Remote Sens.* 33 (2) (1995) 293–304, <https://doi.org/10.1109/TGRS.1995.8746010>.
- [20] F.R.S. Karl Pearson, LIII. On lines and planes of closest fit to systems of points in space, *The London, Edinburgh, and Dublin Philosophical Magazine and Journal of Science* 2 (11) (1901) 559–572, <https://doi.org/10.1080/14786440109462720>.
- [21] Y. Chen, H. Jiang, C. Li, X. Jia, P. Ghamisi, Deep Feature Extraction and Classification of Hyperspectral Images Based on Convolutional Neural Networks, *IEEE Trans. Geosci. Remote Sens.* 54 (10) (Oct. 2016) 6232–6251, <https://doi.org/10.1109/TGRS.2016.2584107>.
- [22] E. Chen, X. Wu, C. Wang and Y. Du, “Application of Improved Convolutional Neural Network in Image Classification,” 2019 International Conference on Machine Learning, Big Data and Business Intelligence (MLBDBI), 2019, pp. 109–113, doi: 10.1109/MLBDBI48998.2019.00027.
- [23] G. Lou, H. Shi, Face image recognition based on convolutional neural network, *China Commun.* 17 (2) (Feb. 2020) 117–124. <https://doi.org/10.23919/JCC.2020.02.010>.
- [24] M. Sabokrou, M. Khalooei, M. Fathy, E. Adeli, Adversarially Learned One-Class Classifier for Novelty Detection, *IEEE/CVF Conference on Computer Vision and Pattern Recognition* 2018 (2018) 3379–3388, <https://doi.org/10.1109/CVPR.2018.00356>.
- [25] F. Pedregosa, G. Varoquaux, A. Gramfort, V. Michel, B. Thirion, O. Grisel, M. Blondel, P. Prettenhofer, R. Weiss, V. Dubourg, J. Vanderplas, A. Passos, D. Cournapeau, M. Brucher, Matthieu Perrot, Édouard Duchesnay 12 (85) (2011) 2825–2830. <https://arxiv.org/abs/1201.0490>.